

TSUNAMI HAZARD ASSESSMENT FOR PERMANENTLY MOORED FSRU MARINE TERMINAL IN CHILE

by

Eric Smith¹, P. Lynett² and C. Rodriguez³

1 ABSTRACT

Evaluation of tsunami effects on moored vessels is not typically considered in marine terminal design due to the low probability of a vessel calling at a terminal simultaneously with a design-level tsunami event. A methodology is needed for permanently moored floating LNG storage and regasification units (FSRUs) in tsunami hazard areas like Chile. The authors present an innovative method for developing a design tsunami hazard assessment for permanently moored vessels consistent with other considered hazards (e.g. seismic) which may be used for terminal design.

2 INTRODUCTION

Chile has a long history of great subduction zone earthquakes and the local tsunamis produced by them. Since the 1500's, there have been 14 documented earthquakes with Mw greater than 8.0, including the 1960 Mw 9.5 Valdivia earthquake, the largest recorded earthquake in recent human history. The Andes LNG project is planned to store and regassify liquefied natural gas (LNG) onboard a Floating Storage and Regasification Unit (FSRU) vessel and deliver gas via pipeline to an onshore power plant. Evaluation of tsunamis for moored vessels is not typically considered for terminal design due to the low probability of a vessel calling at a terminal simultaneously with a design-level tsunami event. However, in the case of a FSRU, the vessel is on site continuously for 20 years or more, greatly increasing the probability of the moored vessel occupying the berth during a tsunami event. A methodology is needed for permanently moored floating LNG storage and regasification units (FSRUs) in tsunami hazard areas like Chile.

In the immediate vicinity of the project site, the earthquake of 1922 generated the largest recent tsunami, with a likely amplitude of 3m near the proposed terminal. In this paper, we present a tsunami hazard assessment approach to account for the great tsunamis generated by these local earthquakes, and the potential effects of this hazard on the Andes LNG floating vessels and marine terminal. A two-part approach was employed: First we analyze the propagation and variation of earthquake-generated tsunamis to the project site and evaluate the statistical probability of tsunami impacts; second we evaluate the impact of the tsunami currents and water levels on a moored LNG carrier.

3 PROJECT DESCRIPTION

Figure 1 shows the proposed marine facilities general layout and the single berth sea island jetty layout at the project site in Chascos Bay on the Chilean coast, approximately 650 km north of Santiago. The terminal will consist of a permanently moored FSRU secured by a conventional mooring system of mooring and breasting dolphins at a single berth sea island jetty, supplying gas to a subsea pipeline. The LNGCs will deliver LNG to the FSRU and will berth on a transient basis. The mooring analysis of the terminal assessed two discrete mooring arrangements: Mooring Arrangement A, where the LNGC deploys mooring lines directly to the FSRU; and Mooring Arrangement B, where two additional mooring dolphins (independent of the FSRU mooring system) provide additional breasting lines that connect the LNGC directly to the additional dolphins. Pneumatic fenders will be located between the LNGC and FSRU vessels and will be connected to the FSRU.

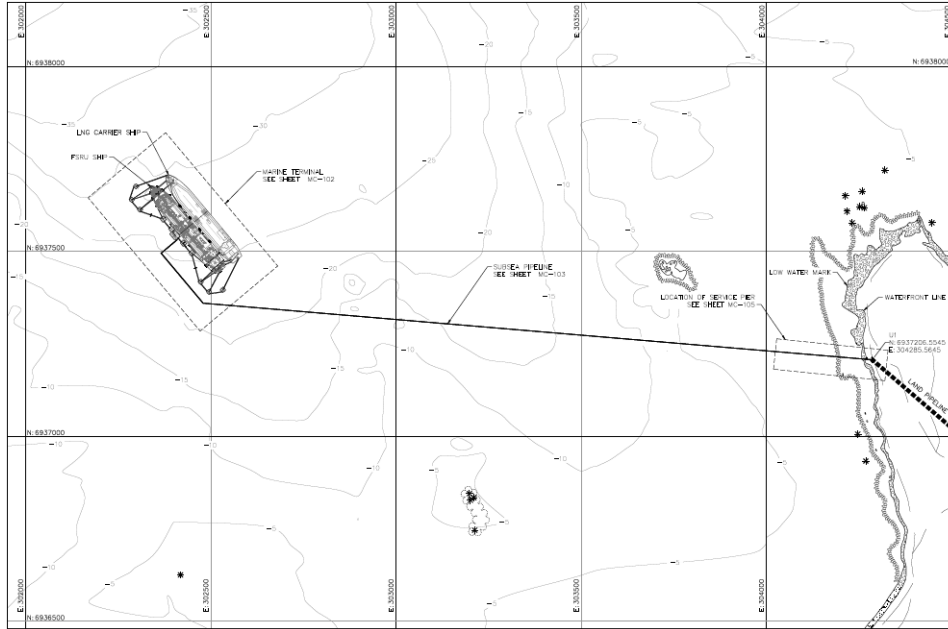


Figure 1 Project Site

4 TSUNAMI MODELING

For the work presented here, two different model suites are used. Each tsunami event is simulated with both modeling approaches. The purpose of using two different modeling suites is to confirm confidence in the models' accuracy with respect to the complex wave components and directions that exist along the Chilean coast during a tsunami. Furthermore, each simulation can be considered as a separate realization of a potential tsunami, adding to the statistical database of tsunami currents for use in the mooring analyses.

4.1 Simulation with Coupled COMCOT+COULWAVE

For the large-scale, regional propagation, the nonlinear shallow water model COMCOT is employed. Following Son et al. (2011), in the nearshore area where site-specific predictions are desired, COMCOT is coupled with the Boussinesq-type model, pCOULWAVE. pCOULWAVE then provides a detailed simulation of tsunami elevations and currents, with a resolution of approximately 10 m. Details about the models are provided below.

COMCOT is a well-established model for tsunami studies, and accurately predicts tsunami propagation. COMCOT solves the nonlinear shallow water wave equations in conservative form with the added effect of bottom friction. Bottom friction is formulated with a Mannings "n" coefficient. The numerical scheme employed by COMCOT is the explicit leap-frog difference method. Nonlinear terms in the model are approximated with upwind finite differences and linear terms by two-point centered finite differences. This numerical scheme is stable and robust but is a low-order accurate method, meaning that it is susceptible to numerical dispersion and dissipation errors. Physically, this implies that nearshore currents, where jets and eddies are important, may not be predicted properly with this model; such features may be overly damped due to numerical dissipation.

To generate the tsunami from an undersea earthquake, COMCOT uses the fault model of Okada (1985). The main assumptions of this model are a rectangular fault plane within an elastic deformation. The fault model predicts the deformation of the seafloor, which corresponds directly to the initial deformation of the ocean water free surface. Once the earthquake has been described with the above parameter set, COMCOT is able to propagate the initial disturbance across oceans.

pCOULWAVE solves the Boussinesq-type equations in conservative form, including turbulent viscosity and the associated horizontal and vertical vorticity terms (Lynett 2006, 2007; Lynett et al., 2010). Bottom friction in this study is also expressed with a Mannings “n” coefficient. The numerical method uses a fourth-order monotone upstream-centered schemes for conservation laws–total variation diminishing (MUSCL-TVD) to solve the leading order (shallow water) terms, while for the dispersive terms, a cell averaged finite volume method is implemented. For the time integration, a third order Adams–Bashforth predictor and the fourth-order Adams–Moulton corrector scheme has been used to keep numerical truncation errors small.

4.2 Simulation with MOST

Earthquake-generated tsunamis, with their long wavelengths, are ideally matched with Non-linear Shallow Water (NSW) for transoceanic propagation. Models such as those by Titov and Synolakis (1995) and Liu et al. (1995) have been shown to be reasonably accurate throughout the evolution of a tsunami and are in widespread use today. At present, the Method of Splitting Tsunami (MOST) hydrodynamic model is implemented. MOST was introduced by Titov and Synolakis (1995 and 1998). This model has been extensively validated and used for tsunami hazard assessments in the United States and is currently maintained and in operational use at National Oceanic and Atmospheric Administration / Pacific Marine Environmental Laboratory (NOAA/PMEL). Variants of the MOST model have been in constant use for tsunami hazard assessments in California since the mid 1990s. MOST solves the NSW equations using a wave-characteristic solver approach (Titov and Synolakis, 1998). The numerical scheme uses a second-order differencing approach for both linear and nonlinear terms, and bottom friction is included using the same Manning’s roughness formulation used by COMCOT. To generate the tsunami from an undersea earthquake, MOST uses the fault model of Okada (1985), again just as with COMCOT.

4.3 Tsunami Model set up

The bathymetry/topography for the simulations is taken from different sources for the two different models. For the regional simulations performed by COMCOT, the bathymetry and topography are taken from the GEBCO database, using 2 arc-minute global bathymetry and topography. An image of the bathymetry map used for these simulations is shown in Figure 2. The pCOULWAVE domain is a much smaller area, centered on the site location. The data used to generate this bathymetry grid was provided in the form of depth contour lines, and these were interpolated to create a numerical grid with constant grid length of 10 meters.

The wave enters the pCOULWAVE domain through the offshore boundaries. The information about this incoming wave is provided by the COMCOT simulation. This coupling is one-way, in that pCOULWAVE receives boundary information from COMCOT, but not vice-versa. This is a common and efficient coupling technique when dealing with model domains that vary widely in grid resolutions.

Dissipation is included in the pCOULWAVE simulation through bottom friction and wave breaking. Bottom friction is modeled via a Mannings friction formulation, using a bottom roughness value of $0.025 \text{ m}^{1/3}$, which is a value commonly used for long waves in shallow waters, and conservatively represents a relatively smooth seafloor. Wave breaking is approximated through the equations developed for and included in the pCOULWAVE model, which have been shown to be accurate for a wide range of field cases.

The pCOULWAVE simulations are executed using a horizontal resolution of 10 m on a grid of 1,500 by 1,000 grid points in the x (east-west) and y (north-south) directions respectively. Each simulation is run for 400 minutes of physical time. Thus, the simulation domain is composed of 1.5 million grid points, and the duration is covered by 475,000 time steps (400 minutes of simulation time, using a time step of 0.05 seconds). Boussinesq-type simulations tend to be computationally demanding, and the simulations presented here are run on a large cluster to make use of parallel processing, each requiring about 40 hours of wall clock time on 120 processor cores.

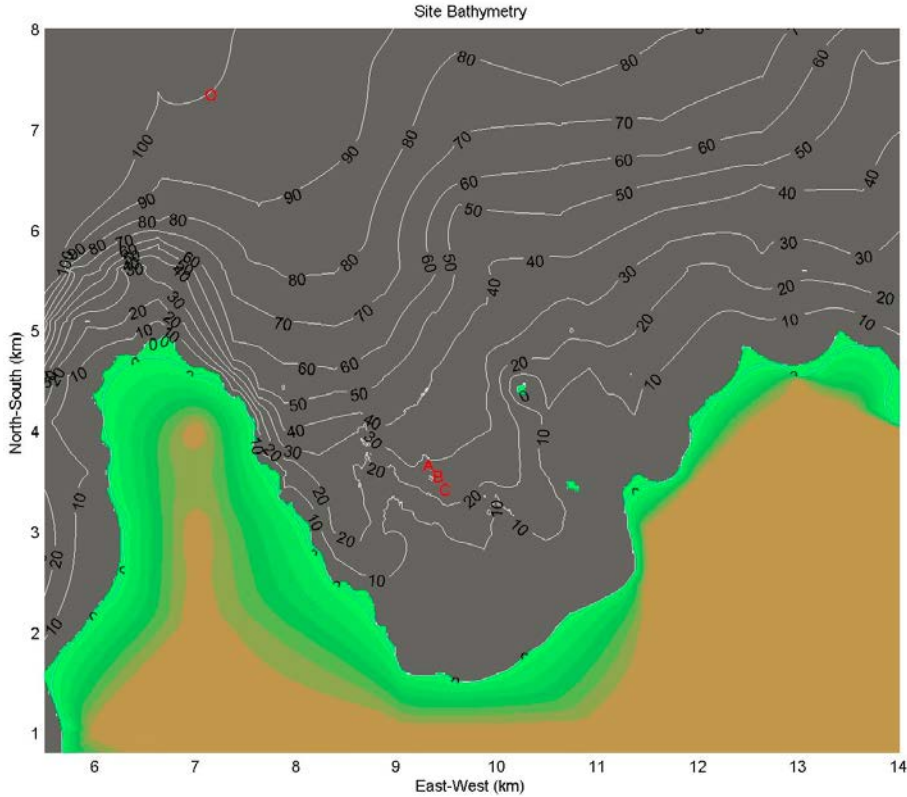


Figure 2 Bathymetry and Topography of the Study Area

For the MOST simulations, the tsunami waves were propagated across the SE Pacific Ocean through the same bathymetric grid used by COMCOT. In the finite-difference scheme employed in MOST, the changes in the tsunami as it travels into shallower water are accounted for by using three nested grids of increasing spatial resolution. The coarsest grid which covers the largest area has 12 arc-sec resolution, whereas the intermediate and finest grid have 3 arc-sec and 1/3 arc-sec (~10m) spatial resolution respectively. The coarse and intermediate grids were obtained by interpolating the 2014 GEBCO 30 arc-sec global relief dataset. The high resolution DEM for this study is identical to that used by pCOULWAVE and described above. Bottom friction is modeled using the same Manning's "n" coefficient as used in the COMCOT+pCOULWAVE approach

4.4 Design Scenarios

To provide a range of potential tsunami impacts at the design site, five different earthquake scenarios are examined with properties given in Table 1. These earthquake properties are provided by the seismic report (Comte and Ortega, 2015). These earthquake scenarios are chosen for study as they represent that largest known earthquakes in the local area.

Year	M _w	Fault Length [km]	Fault Width [km]	Rupture Area [km ²]	Average Slip [m]
1922	8.5	400	100	40,000	4.8
1730	8.7	450	80	36,000	10.60
1943	8.0	220	80	17,600	1.93
2015a	8.3	220	80	17,600	5.44
2015b	8.3	250	70	17,500	5.48

Table 1: Earthquake Properties of Tsunami Scenarios

In this section, the COMCOT+pCOULWAVE model is used. While simulation results will be discussed in detail in this section, first, a summary table showing the primary results from each earthquake scenario is provided. This data is given in Table 2 and Table 3 below, which shows the arrival time of the initial sea level change due to the tsunami, and the ranges in the maximum water level, minimum water level, and maximum speed at the design site. It is clear that the 1922 event, which is controlled by an earthquake in the immediate vicinity of the design site, controls all aspects of the tsunami hazard.

Source	Arrival Time Post-Earthquake of first 5 cm sea level change (minutes)	Arrival Time Post-Earthquake of the first tsunami crest (minutes) and its elevation (m)	Range of Predicted Maximum and Minimum Water Levels along Berth (meter w.r.t. MSL)
1922	4	14 min / +2.9 m	2.8 to 2.9 -3.2 to -3.4
1730	41	51 min / +0.6 m	1.2 to 1.3 -1.1 to -1.3
1943	36	43 min / +0.1 m	0.16 to 0.18 -0.15 to -0.16
2015a	36	45 min / +0.3 m	0.40 to 0.48 -0.41 to -0.42
2015b	35	45 min / +0.3 m	0.43 to 0.49 -0.50 to -0.51

Table 2: Summary of Tsunami Elevation from Scenario Simulations

Source	Current Associated with the First Tsunami Crest (m/s)	Range of Predicted Maximum Tsunami Current along Berth (m/s)
1922	1.2	2.0 to 2.6
1730	0.19	1.1 to 1.4
1943	0.03	0.35 to 0.40
2015a	0.10	0.58 to 0.65
2015b	0.10	0.41 to 0.56

Table 3: Summary of Tsunami Currents from Scenario Simulations

4.5 Tsunami Stochastic Approach

To provide tsunami hazard information for the FEED level design, a “stochastic scenario” approach is used that allows for the approximate expression of tsunami recurrence periods. From the five scenario simulations discussed above, it is clear that the 1922 earthquake source leads to the greatest tsunami impacts at the site; therefore, it corresponds to the design earthquake for tsunami hazard. With information provided in the scientific literature (Comte and Ortega, 2015), it is expected that a 1922-like earthquake (i.e., Mw 8.5 with rupture immediately offshore of the site) occurs once every 100-250 years. However, while the earthquake has this recurrence period, we cannot immediately assign this return period to the tsunami effects simulated by this source. The earthquake recurrence period is a function of its magnitude only, and other parameters, such as focal depth and internal rupture angles, while controlling the initial tsunami properties, play no role in this return period. Therefore, to quantify a tsunami recurrence period, we must understand the range of potential tsunami impacts that might be caused by different configurations of a Mw 8.5 earthquake offshore of the site.

The following set of tsunami simulations, each with a slightly different source condition, is performed:

1. A “baseline” earthquake, with best-estimated earthquake parameters (epicenter location, focal depth=15km, strike=0 degrees, dip=20 degrees, and rake=90 degrees) for a local Mw 8.5 earthquake, as provided by the seismic report (Comte and Ortega, 2015).
2. Shift epicenter to south by 25% of rupture length from “baseline” earthquake
3. Shift epicenter to north by 25% of rupture length from “baseline” earthquake
4. Shift epicenter to south by 50% of rupture length from “baseline” earthquake
5. Shift epicenter to north by 50% of rupture length from “baseline” earthquake

6. Shift epicenter to east by 25% of rupture width from “baseline” earthquake
7. Shift epicenter to west by 25% of rupture width from “baseline” earthquake
8. Use focal depth of 10 km with “baseline” earthquake
9. Use focal depth of 20 km with “baseline” earthquake
10. Use focal depth of 25 km with “baseline” earthquake
11. Change strike angle to 12 degrees from “baseline” earthquake
12. Change strike angle to 6 degrees from “baseline” earthquake
13. Change Dip angle to 17 degrees from “baseline” earthquake
14. Change Dip angle to 23 degrees from “baseline” earthquake
15. Change Rake angle to 102 degrees from “baseline” earthquake
16. Change Rake angle to 78 degrees from “baseline” earthquake

As noted previously, the parameters changed in this list represent quantities that can affect the tsunami significantly, but play no direct role in the quantification of earthquake magnitude. The range of these values are taken from recent large earthquakes in the region. While there are no available distributions for these values, which would be needed for a robust probabilistic analysis, it is reasonable to assume the distributions, within the values tested, resemble white noise distributions. Thus, each of the simulations tested has an equal chance of occurring; i.e., each of these scenarios has an equal chance of being the next Mw 8.5 earthquake to occur in this area.

All 16 scenarios were simulated by both modeling suites (i.e., the COMCOT/COULWAVE suite and the MOST suite), therefore, 32 different simulations are included in this analysis. For each of the simulations, the speed versus direction polar plots are generated for the berth location. Using the polar plots for each of the 32 simulations, probability of exceedance curves for maximum simulated speed as a function of direction can be generated. To perform this analysis, current heading was divided into 2-degree bins, and an exceedance curve developed for each bin. As there are 32 simulations, each exceedance curve is composed of 32 points. With this information, it becomes possible to express the relative likelihood of a specified current-direction pair, in terms of useful recurrence periods. For example, if the design earthquake for tsunami hazard is assumed to have a return period of 250 years, and a speed of 2 m/s (at a specific heading) is only exceeded in half of the tsunami simulations, then this information can be combined to state that a speed of 2 m/s (again, at this specific heading) will only be exceeded, on average, every 500 years. Similarly, a speed that is only exceeded in one out of every 10 simulations, or equivalently a 10% exceedance probability, would have a recurrence period of 2,500 years.

Figure 3 provides the maximum speed as a function of direction for three different exceedance levels. What is immediately clear is that, with decreasing exceedance level, or increasingly rare currents, the polar speed distribution becomes wider in the broadside direction. The physical reason for this “fattening” of the broadside current distribution is that eddies are present in this area. While these eddies exist in all of the simulations, then tend to occur in a chaotic fashion across the realizations, yielding a random but widely spread direction. Such a process is a primary motivating factor for this type of statistical analysis, where a single deterministic simulation might not provide a complete description of the potential variability of this complex velocity field.

The mooring analysis of the vessel targets a specific tsunami recurrence period or periods. To this end, it is necessary to assign each simulation a best-match exceedance value. This is performed by determining which simulation produces a maximum speed envelope that best matches the envelope for a specific exceedance level. Figures 4 and 5 provide these best-match scenarios for exceedance values of 10% and 50%, respectively. The best match is shown on the left, and the second best match on the right; black lines show the simulation time series, and the red lines the exceedance envelope.

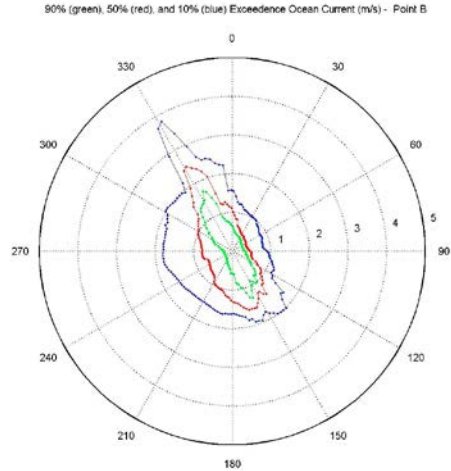


Figure 3: Maximum Tsunami Speed as a Function of Direction for Three Different Exceedance Levels

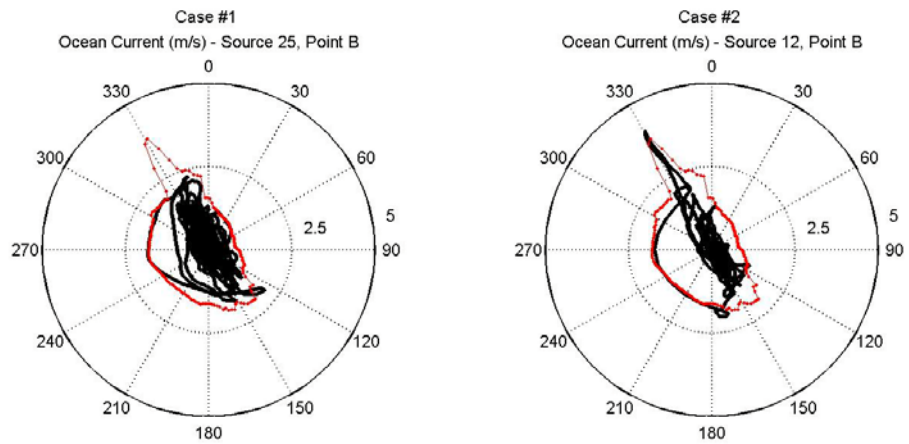


Figure 4: Best-Match Scenarios 10% Speed Exceedance Envelope from the Entire 6-Hour Simulation

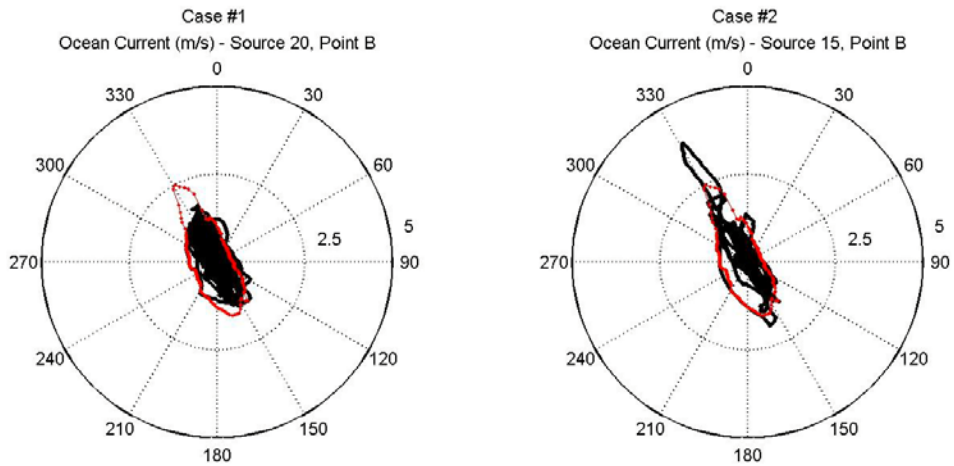


Figure 5: Best-Match Scenarios 50% Speed Exceedance Envelope from the Entire 6-Hour Simulation

4.6 Duration of Tsunami Events

In addition to the design exceedance level, the design duration is an important parameter. For this project, we determine exceedance envelopes based on simulation data from the first 60 minutes of the event, the first 90 minutes of the event, and the entire 6 hours of the simulation. From inspection of these envelopes, it is evident that the maximum currents along the 330-150 degree axis are insensitive to the design duration. The reason for this is that these currents are associated with the first waves of the event, occurring within the first hour. However, it is also evident that as the design duration increases, the off-main-axis currents grow significantly. This is due to the existence of eddies, which can create currents in any direction. Eddies take time to be generated and evolve, and thus are not a strong forcing during the early times of the event.

From comparison of the current predictions between the MOST and COMCOT+pCOULWAVE results, it is evident that the two approaches yield different behaviors for eddies. The current vs direction distributions for the MOST results tend to show relatively large on-axis (330-150 degree axis) currents and relatively small off-axis currents. The COMCOT+pCOULWAVE results, on the other hand, yield the opposite trends, with relatively low on-axis and relatively high off-axis currents. The reason for this difference lies in the physics of the two approaches, or more specifically the turbulence closure found in pCOULWAVE compared to that in MOST. The pCOULWAVE model includes various turbulent and rotational corrections, designed specifically to handle complex coastal currents created by tsunamis (i.e. Son et al., 2011). The manifestation of these physics results in dispersion of the current field in all directions through the generation and evolution of eddies. While the MOST model does predict the creation of eddies, the behavior of these features is different between the two models. As there is little data to demonstrate which model is a better predictor of currents for this particularly site, allowing realizations from both models to have equal weighting permits both relatively large on-axis and relatively large off-axis currents to be included in the analysis.

5 TSUNAMI MOORING ANALYSIS

The performance of the moored vessels was assessed by running a series of dynamic mooring analyses of the tsunami events. The design basis for the terminal specifies that the FSRU shall be capable of departing berth in an emergency. However, in order to investigate the effects on mooring infrastructure in case of having a moored vessel, the dynamic mooring simulations are conducted for two scenarios: the FSRU at the berth by itself; and the FSRU and LNG carrier in ship-to-ship (STS) transfer operations. Performance results of both the LNGC and FSRU mooring are predicated on departing berth within 60 minutes and 90 minutes, respectively, of the earthquake-generated tsunami event.

We selected tsunami events for the mooring analyses based on the combined return period of the earthquake event and the current exceedance threshold acceptable for the design of the berth. The FSRU-only mooring arrangement is simulated for the first 90 minutes of the 10% exceedance tsunami (return period of 1000-2500 years). The STS mooring arrangement is simulated for the first 60 minutes of the 50% exceedance tsunami (return period of 200-500 years).

5.1 Mooring Arrangements

The FSRU mooring arrangement, presented in Figure 6, consists of 22 mooring lines with 22 m polypropylene tails. There are sixteen (16) breasting lines and six (6) spring lines. All lines were modeled as Samson Amsteel Blue mooring lines, a high modulus polyethylene (HMPE) rope. For the FSRU Mooring Arrangement, the vessel was modeled at loaded draft condition, as the induced tsunami current loads associated with the loaded draft condition are assumed to be greater than those associated with the ballast draft condition. This is due to the greater submerged area of the loaded draft condition, relative to the ballast draft condition.

The primary mooring arrangement analyzed for the STS consistent of a LNGC is moored exclusively to the FSRU, presented in Figure 7. The analysis included separate analyses of the LNGC in ballast and loaded draft conditions. For analysis cases where the LNGC was modeled in ballast, the FSRU was modeled as loaded, and vice-versa. The STS Mooring Arrangement has twenty-two (22) mooring lines dedicated to the

FSRU (identical to the FSRU only mooring arrangement) and sixteen (16) ship-to-ship lines. Of these STS lines, ten (10) are breasting lines and (4) are spring lines. Four (4) fenders were modeled between the vessels. These fenders are fixed to the FSRU, and are spaced equivalently along quarter-points of the hull's broad, flat side area. The numbering scheme associated with Mooring Arrangement A is presented in Figure 7.

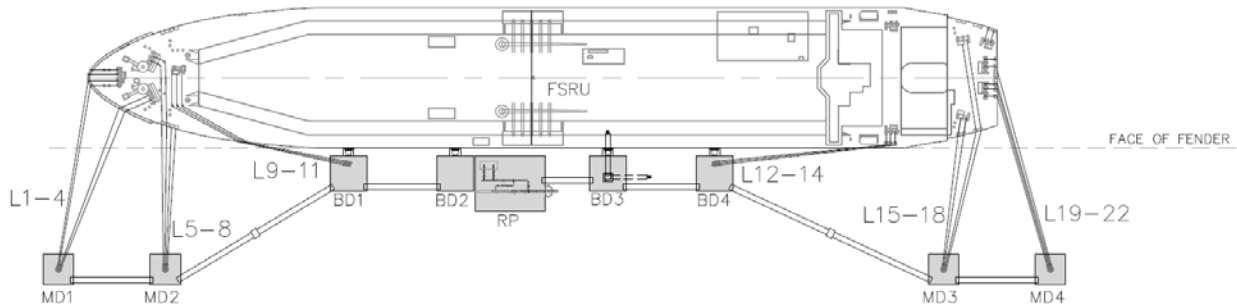


Figure 6: FSRU Only Mooring Arrangement

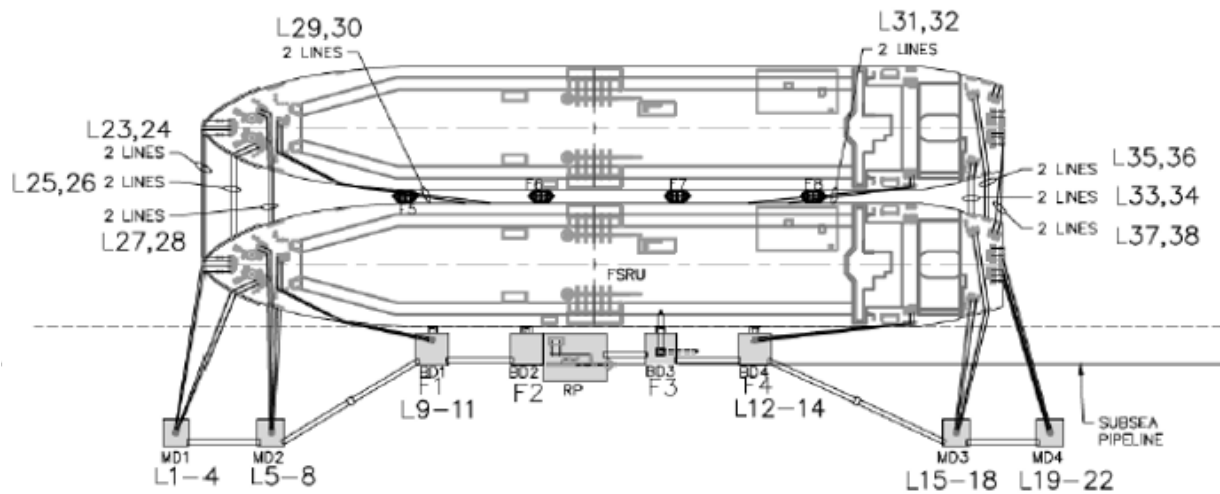


Figure 7: Mooring Arrangement for STS transfer

5.2 Analysis Software

The AQWA suite of software was used to model the dynamic response of the FSRU and LNGC mooring. AQWA comprises a suite of programs that performs three dimensional diffraction/ radiation analysis and calculates first order and second order (non-linear drift) forces on fixed or floating bodies. The submerged body surface is described by a finite element mesh. The software can resolve multiple floating bodies simultaneously as well as fixed structures. The model computes the hydrostatic and frequency response of the moored structures as well as hydrodynamic interactions between the floating structures and calculates the added mass and damping matrices for the floating bodies.

5.3 Modeling Assumptions

5.3.1 Mooring Line and Fender Stiffness Modeling

The load-deflection response of a mooring line and tail combination or a fender can be described by a polynomial function. Fifth order stiffness polynomials were input into the dynamic models to define the responses of mooring lines and fenders within the system. Similarly, fender stiffness polynomials describe the response of the fenders within the model, and are based on force/deflection data provided by the fender manufacturer.

For each vessel, a mesh panel model was created; this panel model provides the definition of the vessel's hull for the AQWA radiation/diffraction and time-domain analyses. Figure 8 presents the side-by-side model of hull meshes.

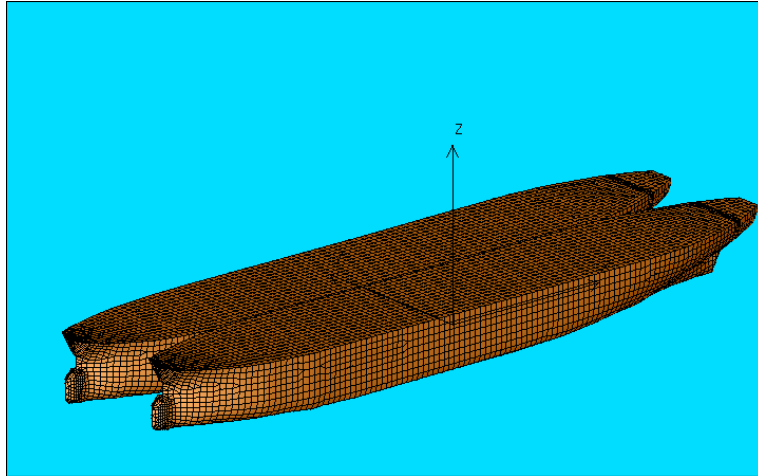


Figure 8: Panel Mesh AQWA Model of STS Transfer

5.3.2 Water Elevation Changes

AQWA modeling framework does not allow for changes of the baseline water level (except for waves) during a time-domain simulation. In order to account impact of changes of water level during the tsunami event, additional line stresses due to fluctuations of the water surface elevation were calculated and added to the mooring response. Each time-step in the tsunami time series applied to the model has a corresponding water surface elevation. As the elevation increases, mooring lines experience greater extension and, therefore, greater tensions. The additional forces from these effects were determined by assessing the additional extension of each line at every time-step and determining the corresponding increases in tension from the developed mooring line stiffness curves. These increases in tension were added to the tensions due to the tsunami current loads for each time-step during post processing of the AQWA simulation results.

5.3.3 Dynamic Response in Heave

Due to the long periodicity of the tsunami event (characteristic wave period on the order of 900 seconds), it is assumed that there is a negligible dynamic response in heave for both the FSRU and STS analysis cases, and that the vessels' response is quasi-static.

5.3.4 Modeling Tsunami Data in the AQWA Time Domain

The wind and current forces calculated within the AQWA time domain are derived from vessel-specific wind force and current force coefficients in conjunction with the current speeds defined within the time-history. The force coefficients are defined in units of force per velocity-squared (for either wind or current velocities).

Conventionally, AQWA only accommodates wind-speed time-histories, and does not have an input option for current-speed time-histories. This limitation was circumvented by defining the tsunami current time-history data as a wind time-history within AQWA; accordingly, the current force coefficients were duplicated and input in the wind force coefficient data category, replacing the wind force coefficients. While both the current speeds and current force coefficients occupy the analogous wind data categories, this method effectively replicates the current forces experienced by the vessels in the tsunami event by applying the current speeds from the time-history to the current force coefficients.

The input of wind force coefficients would be extraneous to the tsunami event analysis, as wind forces are not considered in conjunction with the tsunami event. Therefore, the duplication of the current force coefficients in the analogous wind data category is acceptable for this analysis.

Furthermore, the current forces resulting from drag between the vessels and the water during vessel translations are accounted for by the definition of the current coefficients in their conventional data category.

5.4 FSRU Analysis Criteria

The FSRU mooring arrangement was assessed for adequate response to mooring forces in the lines and fenders. For the tsunami events, FSRU mooring lines were evaluated for limits of both 60% and 80% of their minimum breaking load (MBL). These limits assume the FSRU winch brakes will perform within the range of the manufacturer's specifications. All fenders are required to not exceed the reaction ratings supplied by the manufacturer.

5.4.1 FSRU Analysis Cases

The best-match case that corresponds to the Q10 threshold conditions was applied to the FSRU mooring arrangement for 1.5 hours. The maximum current in the Q10 case is 3.86 m/s.

5.4.2 Mooring Line Tensions

Figure 9 presents the maximum FSRU mooring line tensions for the Q10 event. All of the line tensions remained below the criteria of 60% MBL and 80% MBL. Figure 10 provides the mooring line tension time series. These line tensions include the additional line tension resulting from changes in water surface elevation. There are two main peaks in the line tension. The first peak occurs when the vessel is being pushed directly off berth at approximately 2,950 s into the simulation. This also corresponds to the largest change in water surface elevation. The second peak, which is larger in magnitude with a line tension of 559 kN, occurs at 3,255 s into the simulation. At this time, the current reaches its largest speed at 3.85 m/s and pushes the stern 12 degrees off berth. This causes Lines 20, 21, and 22 (all stern breasting lines) to experience the highest line tensions. However, during the first 90 minutes of the Q10 tsunami, all mooring lines remained with SWL.

5.4.3 Vessel Motions

Figure 11 presents the surge, sway, roll, and yaw motions throughout the 90-minute Q10 exceedance simulation. The Q10 exceedance plots show that the maximum motions occur around 3,260 s when the vessel is being pushed directly sternward. This time corresponds to the largest current speed of 3.85 m/s and when the stern is being pushed 12 degrees off berth. The maximum surge and sway motions are 0.9 m and 1.1 m respectively while the roll and yaw are moderate, below 0.5 degrees.

5.4.4 Fender Forces

In the Q10 exceedance case, none of the fenders exceed the fender's rated reaction of 3,325 kN. Figure 12 shows the fender load time series. Fender 1 (fender closest to bow) experiences the largest fender load of 1,583 kN. This peak load occurs when the vessel is pushed off the berth at time 3000 s and then pushed back on berth beginning at 3,463 s.

PIANC-World Congress Panama City, Panama 2018

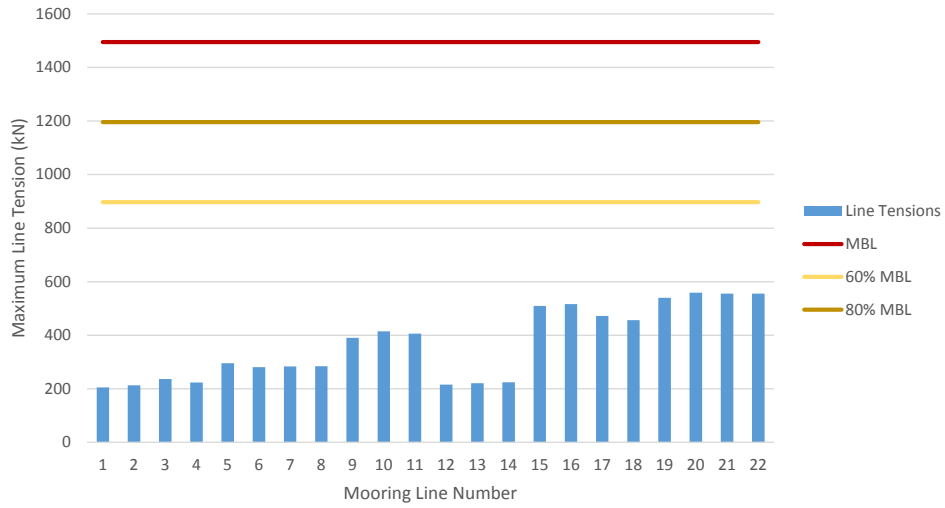


Figure 9: Q10 Maximum Line Tensions

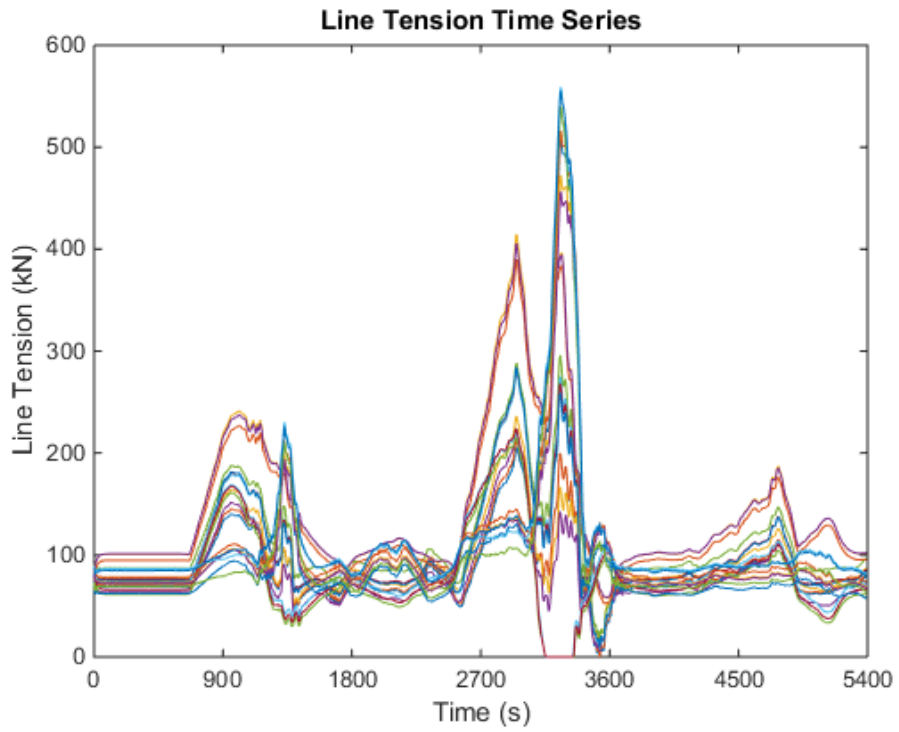


Figure 10: Q10 Line Load Time Series

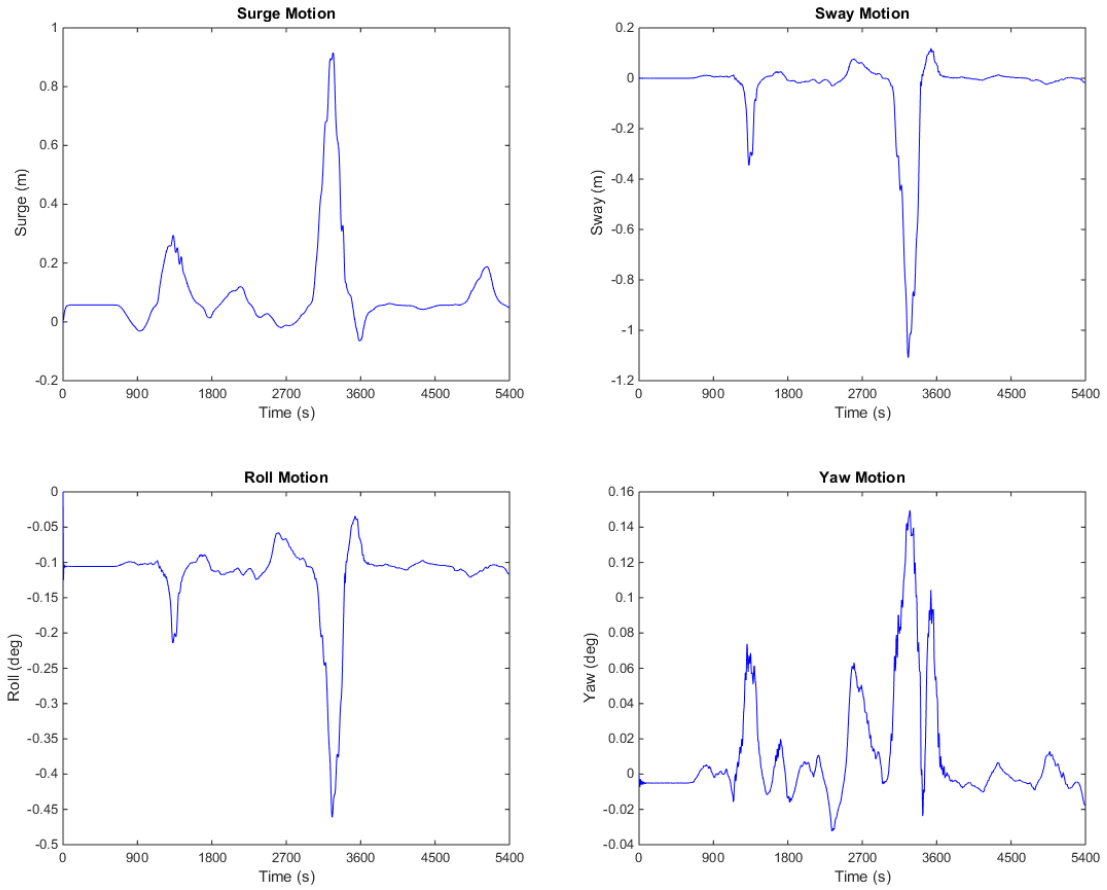


Figure 11: Q10 Surge, Sway, Roll, and Yaw Motion Time Series

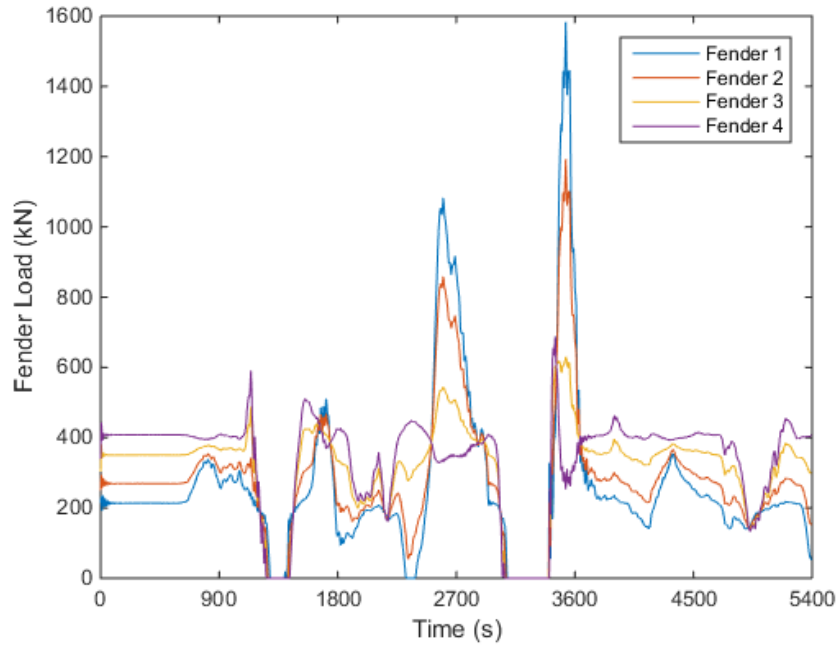


Figure 12: Q10 Fender Load Time Series

5.4.5 Water Elevation Changes

The effect of water elevation changes on mooring line tensions during the tsunami event was examined at 5 second intervals throughout the analysis. For each 5 second interval, mooring line elongations due to the vertical change in water elevation were calculated. The water surface elevations that occur during the Q10 tsunami event are presented in Figure 13. This time-series data is produced during the tsunami simulation process, in addition to current speeds and directions. The corresponding increases in tension due to the fluctuations in water elevation were then calculated and added to the current-force induced tensions to yield the total tension in the system. Note that the maximum total tensions presented in Figure 9 already include both current induced and elevation induced currents.

Figure 13 and Figure 14 show the relationship between the water surface elevation changes and the corresponding increases in tensions for a single spring mooring line. The maximum additional tensions due to water surface elevation change are on the order of 300 kN. These results prove that it is necessary to calculate and add the additional line tension due to water surface elevation changes to the total line tension.

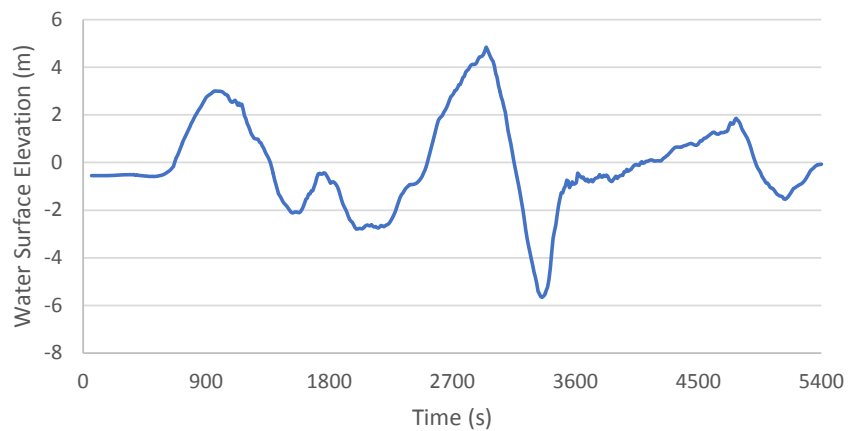


Figure 13: Water surface Elevation of the Q10 Tsunami Event

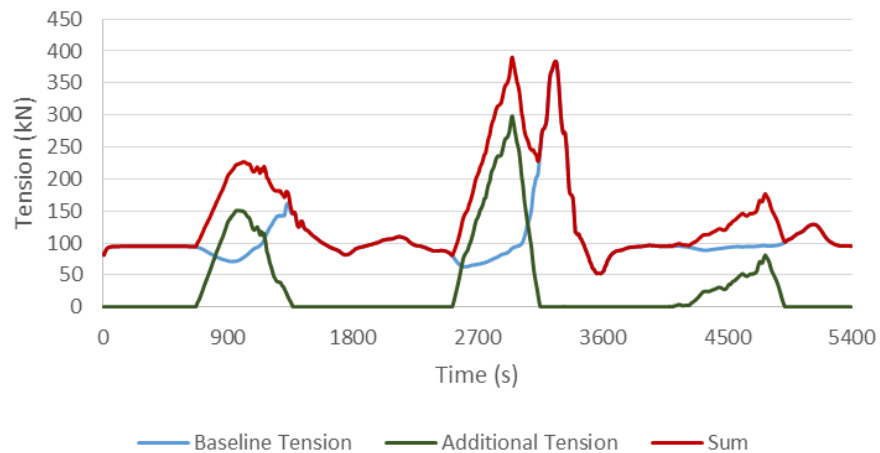


Figure 14: Q10 Superposition of Baseline Tension with Additional Tension Due to Water Surface Elevation Change in Mooring Line 9

5.5 STS Analysis Criteria

For ship-to-ship mooring, the LNGC occupancy will be low (few calls a month and few hours at berth) , therefore the joint probability of both ship being at berth during a tsunami is low. The 50% exceedance (Q50), one hour tsunami event was considered the baseline for the STS analysis.

5.5.1 Q50 Exceedance Tsunami Event

The four design LNGC vessels were analyzed for the Q50 tsunami event for under two mooring arrangements, under both ballast and loaded draft conditions (for analysis cases where the LNGC was modeled as ballast, the FSRU was modeled as loaded, and vice-versa). A total of 16 analysis cases were run for the Q50 tsunami event (4 cases per Design LNGC). Each analysis case yielded time-history data that includes mooring line tensions, vessel motions, and fender compression forces.

5.5.1.1 Mooring Line Tensions

As shown in Figure 15 and **Error! Reference source not found.**, all mooring line tensions remain within the established criteria for all of the FSRU and LNGC mooring lines for the Q50 event. The values depicted represent the maximum mooring line tensions that occur in each line for each Mooring Arrangement, across all FSRU/design LNGC combinations and conditions. Furthermore, these values include the effects of water surface elevation change.

Peak FSRU line tensions (Lines 1-22) appear to be relatively insensitive to mooring arrangement and are well below limiting criteria line tensions. This is expected, as the FSRU mooring lines are sized to resist more onerous exceedance FSRU only cases. The LNGC lines, which are connected ship-to-ship tend to be less optimally placed and therefore more sensitive to the tsunami forcing.

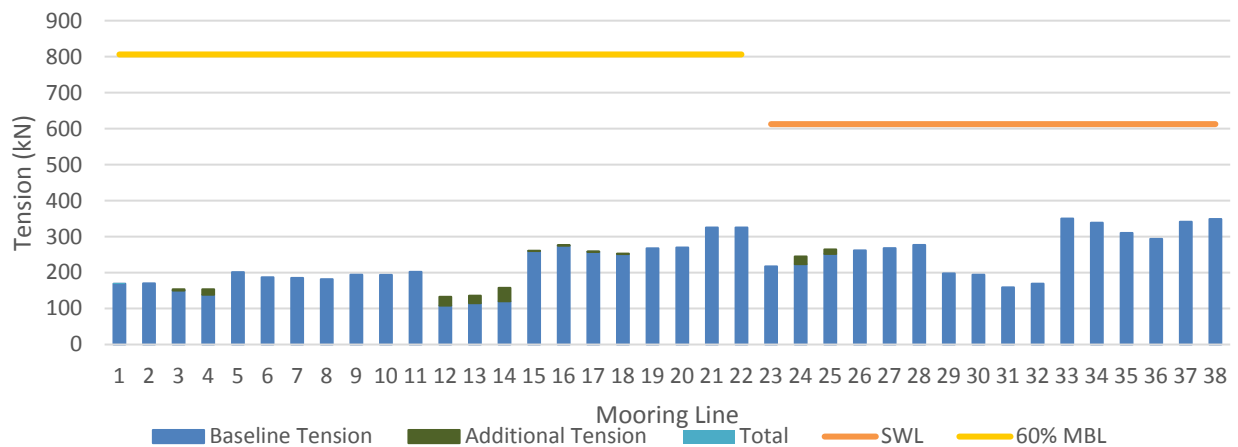


Figure 15: Proportion of Mooring Line Tension Induced by Currents (baseline) and Water Surface Elevation Change (additional)

Maximum LNGC line tensions for both mooring arrangements were below the 50% MBL criteria. The tsunami currents for the Q50 event are approximately aligned with the berth at the peak current speeds, during the initial 60 minutes of the event. Due to the 60 minute tsunami duration used for the FEED analysis and the refined statistical analysis of the tsunami events performed in the FEED tsunami study, the expected yaw motions are reduced due to the relatively narrow angles of peak current loads observed for the Q50 event.

5.5.2 Vessel Motions

The relative vessel motions between the FSRU and LNGC are presented in Figure 16 and Figure 17. These values represent the largest motions of the vessel center of gravity (COG) that occur in any of the 16 analysis cases examined for the Q50 tsunami event. Maximum surge and sway excursions are less than 1.0 m. Note that heave is excluded from the figures. Due to the assumed quasi-static response of the vessels in heave, it is assumed that the COG motions in heave are equivalent to the water surface elevation changes determined by the tsunami event simulation.

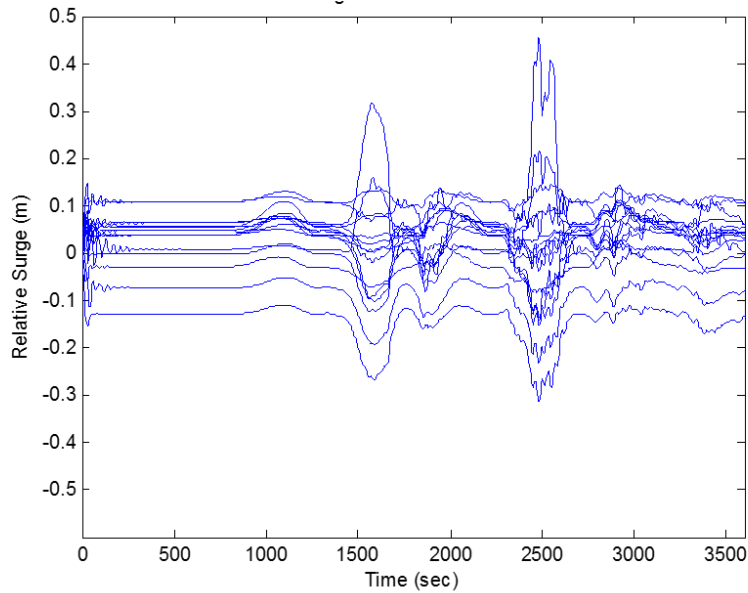


Figure 16: Relative Surge Motion between Vessel COGs; All Q50 Analysis Cases Represented

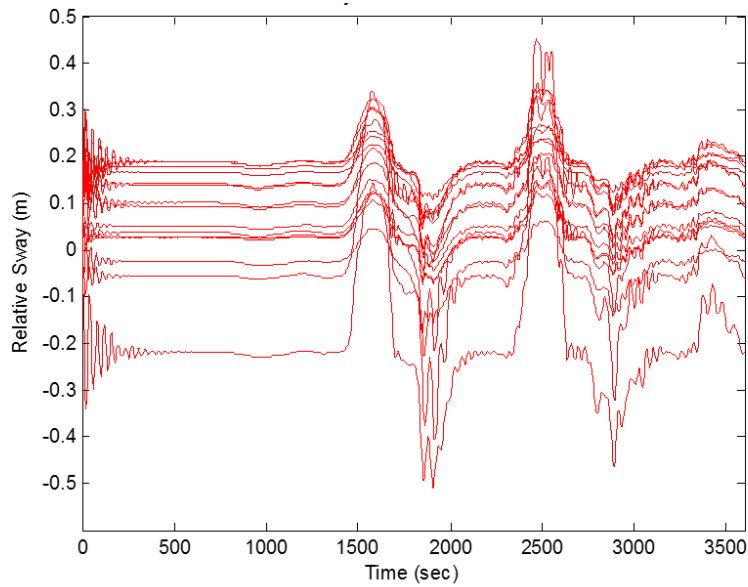


Figure 17: Relative Sway Motion between Vessel COGs; All Q50 Analysis Cases Represented

6 CONCLUSIONS

By combining the tsunami probability evaluation with generation of mooring loads, the mooring performance during tsunami event was predicted to develop an approach for incorporating tsunami mooring loads into the marine structural design.

The tsunami hazard from five different earthquake scenarios was assessed. The numerical tools used for the study include two coupled models, one for the open ocean propagation and another for the site-specific hydrodynamics. The site-specific simulation resolves complex bathymetric features and the associated currents at a horizontal resolution of 10 meters. First, the numerical models are tested against ADCP data measured at the site during the recent 2015 earthquake and tsunami. Although the site is located well north of the rupture zone, a tsunami wave height, or total crest-to-trough distance, of roughly one meter was recorded by the ADCP. The numerical recreation of this event agrees reasonably well with the measured elevation data, with errors between 10-20% in the maximum and minimum elevations. The ADCP recorded no clear velocity signal associated with the tsunami, likely due to under-sampling of the velocity by the instrument.

As expected, the local 1922 source produces the greatest impact at the design location among the five scenarios studied. Measurable waves reach the site just minutes after the earthquake, and the leading crest, which is also the largest predicted for this event at 2.9 m above MSL, arrives 14 minutes post-earthquake. There is very little variation of tsunami elevation along-vessel, less than 10 cm during peak elevation conditions. The speed predictions near the site show considerably more spatial and temporal variation. Maximum predicted speeds along a possible vessel length vary from 2.0-2.6 m/s, and are associated with large eddies (whirlpools) in the immediate vicinity of the site. Due to these eddies and their large spatial changes in flow speed, along-vessel speed gradients may reach 0.5 cm/s per meter of vessel length for periods up to five minutes.

With the simulation of historical tsunamis, it is clear that the 1922 earthquake represents the largest tsunami in the recent past in this area, and is there considered to be the design earthquake for tsunami. To understand the potential variability in the tsunami impacts from this design earthquake, internal parameters of the earthquake are varied and a statistical tsunami analysis is performed. The report provides recurrence periods of the tsunami hazard based on this statistical analysis, which can be used in a mooring line analysis to design to a target reliability consistent with other hazards. The FSRU mooring (without LNGC) meets the allowable mooring criteria for the Q10 level tsunami event during the first 90 minutes of the event. This exceedance level event corresponds to a return period of 1000-2500 years.

Performance results of both the LNGC and FSRU mooring are predicated on departing berth within 60 minutes and 90 minutes, respectively, of the earthquake-generated tsunami event. In the Q10 case, none of the mooring lines reached 60% of their MBL. All of the fenders also stayed below their rated reaction with the maximum fender load (1583 kN) at less than half of the fender's rated reaction. The STS analysis confirmed that the STS mooring arrangements are sufficient in resisting the forces associated for the Q50 threshold tsunami event during the first 60 minutes of the event. This exceedance level event corresponds to a return period of 200-500 years. All FSRU mooring line tensions remained below the criteria of 60% MBL, and all LNGC lines remained below their SWL (50% MBL) with fenders remained within their rated reaction capacity.

This methodology for tsunami impacts on semi-permanently moored structures shows promise for application to other marine terminals in areas with severe tsunami exposure.

7 ACKNOWLEDGEMENTS

The authors wish to thank the engineers Patricio Monardez and Alejandro Pérez, from the Andes LNG team, for their valuable contribution to the development of this work, who through their technical comments and innovative spirit, made it possible to complete the tsunami hazard assessment for this liquified natural gas facility using the approach that was exposed in this document.

8 REFERENCES

- Comte, D. and Ortega, F., 2015, Caracterización Sísmica de la Zona de Ruptura Asociada al Terremoto de 1922 Y Al Terremoto de 1943.
- Lynett, P., 2006, Nearshore wave modeling with high-order Boussinesq-type equations: *Journal of the Waterways and Harbors Division, A.S.C.E.*, v. 132, p. 348-357.
- Lynett, P., 2007, The effect of a shallow water obstruction on long wave runup and overland flow velocity: *Journal of Waterway, Port, Coastal, and Ocean Engineering*, v. 133, p. 455-462.
- Lynett, P., Melby, J., and Kim, D.-H., (2010) "An Application of Boussinesq Modeling to Hurricane Wave Overtopping and Inundation." *Ocean Engineering*, v. 37, p. 135-153. doi: 10.1016/j.oceaneng.2009.08.021
- Okada, Y., 1985. Surface deformation to shear and tensile faults in a half-space. *Bull. Seismol. Soc. Am.* 75, 1135–1154
- Son, S., Lynett, P., and Kim, D.-H. (2011) "Nested and Multi-Physics Modeling of Tsunami Evolution from Generation to Inundation." *Ocean Modelling*, v. 38 (1-2), p. 96-113, doi: 10.1016/j.ocemod.2011.02.007
- Titov, V. V., & Synolakis, C. E. (1995). Modeling of breaking and nonbreaking long-wave evolution and runup using VTCS-2. *Journal of Waterway, Port, Coastal, and Ocean Engineering*, 121(6), 308-316.
- Titov, V. V., & Synolakis, C. E. (1998). Numerical modeling of tidal wave runup. *Journal of Waterway, Port, Coastal, and Ocean Engineering*, 124(4), 157-171.